Acta Crystallographica Section B
Structural Science
ISSN 0108-7681

Structural complexity in minerals: twinning, polytypism and disorder in the crystal structure of polybasite, $(Ag,Cu)_{16}(Sb,As)_2S_{11}$

Michel Evain,[a]* Luca Bindi[b] and Silvio Menchetti[b]

[a]Laboratoire de Chimie des Solides, IMN, UMR 6502 CNRS, Université de Nantes, 2 rue de la Houssinière, BP 32229, 44322 Nantes CEDEX 3, France, and [b]Dipartimento di Scienze della Terra, Università di Firenze, Via La Pira 4, I-50121 Firenze, Italy

Correspondence e-mail: michel.evain@cnrs-imn.fr

Received 25 January 2006
Accepted 15 March 2006

The crystal structures of 222- and 221-polybasite $[(Ag,Cu)_{16}(Sb,As)_2S_{11}]$ crystals have been solved and refined by means of X-ray diffraction data (collected at 100 and 120 K, respectively) from twinned crystals. Both structures consist of the stacking of $[(Ag,Cu)_6Sb_2S_7]^{2-}$ and $[Ag_9CuS_4]^{2+}$ module layers in which Sb forms isolated SbS_3 pyramids typically occurring in sulfosalts; copper links two S atoms in a linear coordination and silver occupies sites with coordination ranging from quasi-linear to almost tetrahedral. An Ag $\rightarrow$ Cu substitution in the $[(Ag,Cu)_6Sb_2S_7]^{2-}$ module layer is observed in both structures, the substitution amount being larger in the 221- than in the 222-polybasite. A pattern of the possible mechanism regulating the type of unit cell that is stabilized is proposed: starting from the hypothetical stoichiometric and fully ordered $Ag_{15}CuSb_2S_{11}$ 222-polybasite structure, with a low $C2/c$ monoclinic symmetry and a large 222 supercell, the disorder introduced by the substitution of Cu for Ag increases the symmetry with a cell reduction along the c axis yielding the 221 supercell and a trigonal crystal system. A further increase of the substitution gives rise to a folding of the cell along the a and b axes and the 111-pearceite structure, space group $P\bar{3}m1$.

1. Introduction

The minerals belonging to the pearceite–polybasite group have been divided into two series (Frondel, 1963; Hall, 1967): one formed by pearceite $(Ag,Cu)_{16}(As,Sb)_2S_{11}$ and antimonpearceite $(Ag,Cu)_{16}(Sb,As)_2S_{11}$, characterized by a 'small' unit cell (labelled 111) and a high Cu content, and one composed of polybasite $(Ag,Cu)_{16}(Sb,As)_2S_{11}$ and arsenpolybasite $(Ag,Cu)_{16}(As,Sb)_2S_{11}$, with double cell parameters (labelled 222) and a low Cu content. In addition, the existence of an intermediate unit cell, labelled 221, for the doubling of the a and b axes only, was claimed by Harris *et al.* (1965), Edenharter *et al.* (1971) and Minčeva-Stefanova *et al.* (1979). These authors observed that the intermediate 221 cell present in some areas of the analysed sample was closely associated with the small 111 cell present in other seemingly identical areas of the same sample. The phase relations occurring in the $(Ag,Cu)_{16}(As,Sb)_2S_{11}$–$(Ag,Cu)_{16}(Sb,As)_2S_{11}$ system were experimentally investigated by Hall (1967), who hypothesized that the variation of Cu content in different samples might play a key role in favouring chemical order–disorder phenomena and, therefore, be the driving force in a different unit-cell stabilization. Recently, Bindi *et al.* (2006) solved the crystal structure of pearceite in the space group $P\bar{3}m1$, by means of a combination of a Gram–Charlier development of

the atomic Debye–Waller factors and a split-atom model (Kuhs & Heger, 1979; Boucher *et al.*, 1992, 1993; Evain *et al.*, 1998). The reason for this unusual approach was linked to the difficulty in efficiently describing the Ag or Cu electron density influenced by the strong ionic conductivity and the mixed occupancies of the atom sites.

In the course of a research project dealing with the structural characterization of silver-bearing minerals from museum collections (Bindi & Cipriani, 2004*a*,*b*,*c*; Bindi *et al.*, 2004; Bindi & Pratesi, 2005), we analysed polybasites in two polybasite-bearing samples with different unit cells.

In this study we report the crystal structure determinations of the 222- and 221-polybasites and discuss the possible mechanisms regulating the type of unit cell that is stabilized.

2. Occurrence and chemical composition

Both samples (Museo di Storia Naturale, Sezione di Mineralogia e Litologia, Università di Firenze, Italy; catalogue numbers 17002/38 and 2503/I for 222- and 221-polybasite, respectively) containing the 222- and 221-polybasite crystals used in the present study are from Hidalgo, Mexico. Polybasite occurs as black anhedral to subhedral grains up to 350 μm in length, and shows a grey–black to black streak. It is worth noting that all the polybasite crystals from sample 17002/38 (five crystals from different areas) checked by means of single-crystal X-ray diffraction gave the 222 unit cell, whereas those from sample 2503/I (four crystals tested) gave the 221 cell.

A preliminary chemical analysis using energy-dispersive spectrometry, performed on the crystal fragments used for the structural study, did not indicate the presence of elements ($Z > 9$) other than S, Cu, Zn, As, Se, Ag, Sb, Pb and Bi. The chemical composition was then determined using wavelength-dispersive analysis (WDS) by means of a Jeol JXA-8200 electron microprobe. Major and minor elements were determined at a 20 kV accelerating voltage and a 40 nA beam current, with 10 s counting time. For the WDS analyses the following lines were used: S $K\alpha$, Cu $K\alpha$, Zn $K\alpha$, As $L\alpha$, Se $L\alpha$, Ag $L\alpha$, Sb $L\beta$, Pb $M\alpha$ and Bi $M\beta$. The estimated analytical precision (in wt%) is: ±0.55 for Ag, ±0.40 for Sb, ±0.30 for Cu, ±0.20 for S, ±0.05 for As and Se, ±0.01 for Zn, Pb and Bi. The standards employed were: galena (S, Pb), Cu pure element (Cu), synthetic ZnS (Zn), synthetic As_2S_3 (As), synthetic $PtSe_2$ (Se), Ag pure element (Ag), synthetic Sb_2S_3 (Sb) and synthetic Bi_2S_3 (Bi). The polybasite fragments were found to be homogeneous within analytical error. The average chemical compositions (eight analyses on different spots), together with ranges of wt% of elements, are reported in Table 1. On the basis of 29 atoms, the formulae can be written as $(Ag_{14.48}Cu_{1.29}Pb_{0.01}Bi_{0.01})_{\Sigma=15.79}(Sb_{1.98}As_{0.09})_{\Sigma=2.07}S_{11.14}$ and $(Ag_{14.27}Cu_{1.69}Zn_{0.03}Bi_{0.01})_{\Sigma=16.00}(Sb_{1.99}As_{0.08})_{\Sigma=2.07}(S_{10.77}Se_{0.16})_{\Sigma=10.93}$ for the 222- and 221-polybasite crystals, respectively.

Table 1
Electron microprobe data (means and ranges in wt% of elements) and atomic ratios with their standard deviations (σ) for the selected 222- and 221-polybasite crystals (17002/38 and 2503/I, respectively).

	wt%	Range	Atomic ratios	σ
222				
Ag	69.22	68.52–70.93	14.48	0.14
Cu	3.63	3.44–3.99	1.29	0.07
Pb	0.09	0.00–0.16	0.01	0.01
Bi	0.10	0.01–0.13	0.01	0.02
As	0.30	0.09–0.44	0.09	0.05
Sb	10.70	10.02–11.14	1.98	0.09
S	15.82	14.99–16.13	11.14	0.11
Total	99.86	99.08–100.36		
221				
Ag	68.15	67.44–69.02	14.27	0.13
Cu	4.76	4.32–5.01	1.69	0.08
Zn	0.09	0.00–0.15	0.03	0.01
Bi	0.09	0.03–0.14	0.01	0.02
As	0.27	0.11–0.35	0.08	0.05
Sb	10.73	10.22–11.01	1.99	0.09
S	15.29	15.09–15.88	10.77	0.12
Se	0.56	0.24–0.85	0.16	0.02
Total	99.94	99.34–100.81		

3. Structure determination

3.1. 222-Polybasite

A rather large crystal was chosen among those tested for the cell parameter doubling (see above). It was fixed at the tip of a glass capillary by means of solvent-free glue. A first data collection was then carried out at room temperature on a Bruker–Nonius Kappa CCD diffractometer using graphite-monochromated Mo K–$L_{2,3}$ radiation. In expectation of a possible crystal twinning, a full diffraction sphere was considered. The diffraction pattern was apparently consistent with a trigonal symmetry, with the a and c parameters doubled ($a \simeq 15.2$ and $c \simeq 24.0$ Å) compared with those of the pearceite structure ($a \simeq 7.4$ and $c \simeq 11.8$ Å; Bindi *et al.*, 2006).

Intensity integration and a standard Lorentz-polarization correction were performed using the Bruker–Nonius *EvalCCD* program package. Subsequent calculations were conducted using the *Jana*2000 program suite (Petricek & Dusek, 2000), except for the crystal-shape and dimension optimization which were performed using *X-shape* (Stoe & Cie, 1996), based on the *Habitus* program (Herrendorf, 1993), and the structure drawings which were realised using the *Diamond* program (Brandenburg, 2001).

The sets of reflections were corrected for absorption *via* a Gaussian analytical method and averaged according to the $\bar{3}m1$ point group ($R_{int} = 0.076$). Starting from the model obtained for the pearceite structure (Bindi *et al.*, 2006) and supposing an $Ag_{15}CuSb_2S_{11}$ stoichiometry, a first averaged structure was looked for in the basic cell ($a \simeq 7.4$ and $c \simeq 11.8$ Å). A residual $R = 0.15$ value was quickly achieved with a large spreading of the silver electron density in the $[Ag_9CuS_4]^{2+}$ pseudo layer (the B layer, see the structure description below). The structure was then extended to a

$2a \times 2b \times c$ cell since the satellite reflections indicate that cell enlargement was stronger than the satellite reflections leading to the doubling of the c parameter. The structure model was subsequently optimized and an ordering sought, but no improvement could be achieved. It was then obvious that the symmetry was not correct and a new structure model was established with different crystal symmetry.

Since the symmetry was previously reported as monoclinic, space group $C2/m$ (Peacock & Berry, 1947; Frondel, 1963; Harris *et al.*, 1965; Hall, 1967), the reflection data set was transformed in the C-centered orthohexagonal cell and averaged accordingly, taking into account the twin law which makes the twin lattice ($\mathbf{L}_T$) hexagonal [twinning by metric merohedry (Nespolo, 2004, and references therein)]. In concrete terms, the only equivalent reflections of the twinned crystal are those related by the inversion operation since $\{E\}$ and $\{\bar{1}\}$ are the only classes of $2/m$ that are complete classes of the first-degree twin polychromatic point group (Nespolo, 2004)

$$K_{\mathrm{WB}}^{(3)} = \left[\bar{3}^{(3)}\,\frac{2^{(2,1)}}{m^{(2,1)}}\right]^{(3)}.$$

For details of the averaging of equivalent reflections for twins in *JANA*2000, see for instance the Appendix in Gaudin *et al.* (2000). Once again, the structure refinement was initiated in the $2a \times 2b \times c$ supercell. A better solution was found (R = 0.08), but with numerous partially occupied sites for Ag in the $[Ag_9CuS_4]^{2+}$ B layer and very large atomic displacement parameters. Since those features could be linked to the doubling of the c parameter, an expansion of the structure in the larger $2a \times 2b \times 2c$ supercell was then realised and a structure model sought. However, no improvement was achieved. Going back to the $2a \times 2b \times c$ supercell, a thorough analysis of the structure (essentially based upon the observation of the very large atomic displacement parameters for particular atoms) suggested that the mirror symmetry element of the $C2/m$ space group should be removed. The reflection and atomic position data sets were then adapted to the $C2$ space group and the structure refined in the $2a \times 2b \times 2c$ supercell. Given the large number of atoms in the starting structural model (more than 150), the site-occupancy refinement of most of the Ag positions, and the use of anisotropic atomic displacement parameters for all the atoms, a severe damping factor (<0.1) was used in the full-matrix refinement and some restrictions among the symmetry-related S atoms in the average cell were set. In addition, to speed up the calculations, the refinements were performed at a $3\sigma(I)$ level for observed reflections and with a $\sin(\theta)/\lambda = 0.7$ Å^{-1} cut-off. A realistic ordered solution could not be found, possibly because of the twin-volume ratios close to 1/3, an incorrect absorption correction, and high correlations between positions and/or atomic displacement parameters.

To further proceed in the structure determination, it was decided to work on a much smaller crystal, then limiting the influence of the absorption correction which cannot be properly accounted for in the presence of large domain twin components. The previously used crystal was then broken into small fragments, two of them being used for new data collections. Both new data sets (full diffraction spheres) were subsequently tested for the structure refinement and led to similar results, except for the twin-volume ratios which differently departed from the 1/3 proportions, thus revealing an inhomogeneous distribution of the twin components throughout the crystal (as opposed to a homogeneous distribution of small domain twin components which would preserve the ratios, whatever the crystal size in the useful range for X-ray single-crystal diffraction). For brevity, only one result is hereafter reported. Using the procedure already presented, the data set was properly converted into an independent monoclinic set ($C2$ space group) and the structure determination resumed with the same drastic conditions. After thousands of cycles, an ordered solution with full site occupations could finally be found by carefully removing atoms with low site occupations and/or non-realistic distances with neighbouring atoms and adding significant positions found in the difference Fourier syntheses. The structure analysis then suggested a higher symmetry with the $C2/c$ space group. After averaging the reflection set accordingly, the structure could be smoothly refined in that symmetry without any damping factor or restrictions. The residual value converged to R = 0.092 for observed reflections [$2\sigma(I)$ level], including all of the collected reflections in the refinement. Analyses of the difference Fourier synthesis maps suggested an additional twin law with a twofold axis, perpendicular to the previous threefold axis, as a generator twin element thus leading to a second-degree twin with the polychromatic point group (Nespolo, 2004, and references therein),

$$K_{\mathrm{WB}}^{(p)} = \left[\frac{6^{(6)}}{m^{(2)}}\,\frac{2^{(2,2)}}{m^{(2,2)}}\,\frac{2^{(2)}}{m^{(2)}}\right]^{(6)}.$$

The introduction of only three new parameters (the new twin volume ratios) dramatically lowered the R value to 0.070, although the new domains being rather small in size [2.07 (3), 0.36 (3) and 4.79 (4)%].

At that stage the inspection of the $F_{\mathrm{obs}} - F_{\mathrm{calc}}$ list revealed a quasi-systematic negative difference for the hkl reflections having $l = 2n + 1$. A second scale factor was then introduced for the satellite reflections leading to the doubling of the c axis. This significantly improved the R value, which was established at R = 0.061. The necessity of a second scale factor is not unusual when dealing with polytypic structures (see, for instance, Nespolo & Ferraris, 2001). It can be related to the lack of accuracy in integrating the intensities of weak and possibly diffuse reflections, linked to small portions of the crystal with the 221 structure (see below).

A non-harmonic approach with a Gram–Charlier development of the Debye–Waller factor up to the third order (Johnson & Levy, 1974; Kuhs & Heger, 1984) was then used to properly describe the electron density of six Ag atoms (*i.e.* Ag3, Ag9, Ag12, Ag14, Ag24 and Ag28), where positive residues were found in the difference Fourier synthesis maps. At the last stage, with anisotropic atomic displacement para-

meters for all atoms and no constraints, the residual value settled at $R = 0.0597$ ($wR = 0.0707$) for 32 369 independent observed reflections [$2\sigma(I)$ level] and 590 parameters and at $R = 0.0967$ ($wR = 0.0731$) for all 43 459 independent reflections.

To improve the structure model, a new data collection was carried out using the same diffractometer at 100 K, the low temperature being achieved by means of an Oxford cryostream cooler. Using the previous room-temperature parameters as a starting point and with the same refinement conditions, the residual value converged to $R = 0.0506$. At that stage the structure analysis showed a particularity for Ag3, having shorter distances than the average Ag—S (see §4), higher U_{eq} value and the need for third-order tensors. All these features suggested a partial occupation of the Ag3 site by Cu atoms, in agreement with the electron microprobe data. By introducing a mixed site occupation for Ag3, the residual value dropped to $R = 0.0501$. Finally, with a secondary extinction coefficient (Becker & Coppens, 1974), the final R value was established at $R = 0.0500$ ($wR = 0.0563$) for 38 764 independent observed reflections [$2\sigma(I)$ level] and 592 parameters and at $R = 0.0650$ ($wR = 0.0575$) for all 43 813 independent reflections. Crystal characteristics, data collection and reduction parameters, and refinement results (100 K only) are gathered in Table 2. Atomic parameters (100 K only) are available in the supplementary data[1] and in Table 3.

It is worth noting that all the atom positions, except those of the Ag atoms in the $[Ag_9CuS_4]^{2+}$ B pseudo layer, approximately follow a mirror (m[010]) symmetry operation. Therefore, through the combination with the c-glide-mirror symmetry operation of the $C2/c$ space group, they are approximately translated by 1/2 along the c axis. Only the Ag atoms in the $[Ag_9CuS_4]^{2+}$ B pseudo layer do not follow that pattern. This feature, along with the absence of the $h0l$, $l = 2n + 1$ systematic extinction because of the twinning, could explain why $C2/m$ was mistakenly thought to be the correct space group and why the structure could not be solved, until now.

3.2. 221-Polybasite

A small crystal was selected among the four crystals tested for the 221 sublattice (sample 2503/I). It was fixed at the tip of a glass Lindeman capillary by means of solvent-free glue. Data collection (full diffraction sphere) was carried out at room temperature using the previously described diffractometer. As for 222-polybasite, the 221-polybasite crystal system appeared as trigonal and could be indexed by a hexagonal cell ($a \simeq 15.1$ and $c \simeq 11.9$ Å) related to that of pearceite by the $2a \times 2b \times c$ relationship. After the usual Lorentz-polarization adjustment and a Gaussian analytical absorption correction based upon optimized crystal shape and dimensions, the structure determination was carried out, starting from the 222-polybasite structure model. Indeed, it was imagined that the 221 structure would approximately correspond to one-half of the unit-cell content of the 222-polybasite structure, that is fulfill the $C2$ symmetry {the hexagonal twin lattice being recovered by a first-degree twin with $[3^{(3)}2^{(2,1)}]^{(3)}$ as the polychromatic point group}. After several refinement cycles it was soon realised, looking at the high parameter correlations and the equal twin

Table 2
Experimental details.

	221-Polybasite	222-Polybasite
Crystal data		
Chemical formula	$Ag_{14.52}Cu_{1.48}S_{11}Sb_2$	$Ag_{14.814}Cu_{1.186}S_{11}Sb_2$
M_r	2256.5	2269.5
Cell setting, space group	Trigonal, $P321$	Monoclinic, $C12/c1$
Temperature (K)	120	100
a, b, c (Å)	15.0954 (12), 15.0954 (12), 11.8825 (8)	26.188 (3), 15.1199 (18), 23.784 (3)
α, β, γ (°)	90, 90, 120	90, 90, 90
V (Å^3)	2344.9 (3)	9418 (2)
Z	4	16
D_x (Mg m^{-3})	6.390	6.401
Radiation type	Mo $K\alpha$	Mo $K\alpha$
No. of reflections for cell parameters	162	228
θ range (°)	6.4–35	6.4–36
μ (mm^{-1})	16.32	16.25
Crystal form, colour	Block, black	Block, black
Crystal size (mm)	0.14 × 0.08 × 0.06	0.15 × 0.12 × 0.09
Data collection		
Diffractometer	Bruker–Nonius Kappa CCD	Bruker–Nonius Kappa CCD
Data collection method	ω, φ	ω, φ
Absorption correction	Gaussian	Gaussian
T_{min}	0.196	0.186
T_{max}	0.417	0.268
No. of measured, independent and observed reflections	102 310, 6847, 6224	144 761, 43 813, 38 767
Criterion for observed reflections	$I > 2\sigma(I)$	$I > 2\sigma(I)$
R_{int}	0.063	0.073
θ_{max} (°)	35.0	36.0
Range of h, k, l	$-24 \Rightarrow h \Rightarrow 24$ $-24 \Rightarrow k \Rightarrow 24$ $-19 \Rightarrow l \Rightarrow 19$	$-43 \Rightarrow h \Rightarrow 39$ $-25 \Rightarrow k \Rightarrow 24$ $-38 \Rightarrow l \Rightarrow 39$
Refinement		
Refinement on	F	F
$R[F^2 > 2\sigma(F^2)]$, $wR(F^2)$, S	0.036, 0.046, 1.41	0.050, 0.057, 1.48
No. of reflections	6847	43 813
No. of parameters	224	592
Weighting scheme	Based on measured s.u.s, $w = 1/[\sigma^2(F) + 0.000484F^2]$	Based on measured s.u.s, $w = 1/[\sigma^2(F) + 0.000484F^2]$
$(\Delta/\sigma)_{max}$	0.001	0.002
$\Delta\rho_{max}, \Delta\rho_{min}$ (e Å^{-3})	1.05, −0.81	1.15, −1.10
Extinction method	B–C type-1 Lorentzian isotropic (Becker & Coppens, 1974)	B–C type-1 Gaussian isotropic (Becker & Coppens, 1974)
Extinction coefficient	0.108 (16)	0.058449

Computer programs used: *JANA*2000 (Petricek & Dusek, 2000).

[1] Supplementary data for this paper are available from the IUCr electronic archives (Reference: LC5045). Services for accessing these data are described at the back of the journal.

Table 3
Higher-order displacement parameters and s.u.s for the selected 222- and 221-polybasite crystals.

Third-order tensor elements C^{ijk} are multiplied by 10^3.

	Ag3/Cu_Ag3	Ag9	Ag12
222-Polybasite			
C^{111}	−0.000034 (13)	−0.000031 (13)	−0.00060 (3)
C^{112}	0.000046 (13)	0.000072 (13)	0.000100 (18)
C^{113}	−0.000018 (8)	−0.000010 (8)	−0.000068 (13)
C^{122}	0.00002 (2)	0.00021 (2)	0.00000 (2)
C^{123}	0.000011 (10)	−0.000032 (9)	0.000030 (11)
C^{133}	−0.000003 (12)	−0.000061 (8)	−0.000012 (11)
C^{222}	0.00022 (9)	0.00019 (6)	0.00030 (6)
C^{223}	−0.00013 (3)	−0.00011 (2)	−0.00006 (2)
C^{233}	0.00010 (2)	−0.000037 (14)	0.000039 (13)
C^{333}	−0.00009 (2)	0.000043 (15)	−0.000014 (17)

	Ag14	Ag24	Ag28
C^{111}	0.000010 (10)	0.000143 (15)	−0.000366 (18)
C^{112}	0.000018 (12)	0.000201 (14)	−0.000067 (14)
C^{113}	0.000005 (6)	−0.000009 (8)	0.000036 (9)
C^{122}	−0.00008 (3)	0.00014 (2)	−0.00002 (2)
C^{123}	−0.000014 (10)	0.000001 (9)	−0.000015 (9)
C^{133}	−0.000016 (7)	−0.000032 (8)	−0.000019 (8)
C^{222}	−0.00334 (16)	0.00014 (6)	0.00004 (6)
C^{223}	0.00011 (4)	0.00003 (2)	−0.000012 (18)
C^{233}	−0.000023 (15)	0.000023 (12)	−0.000008 (12)
C^{333}	−0.000020 (14)	0.000051 (14)	−0.000036 (13)

	Ag3/Cu_Ag3	Ag6	Ag8	Ag10
221-Polybasite				
C^{111}	−0.00041 (12)	−0.00176 (12)	−0.0032 (2)	0.0051 (2)
C^{112}	−0.00011 (10)	−0.00098 (8)	−0.00073 (11)	0.00027 (10)
C^{113}	−0.00007 (8)	0.00017 (6)	0.00112 (10)	0.00057 (10)
C^{122}	0.00051 (12)	−0.00073 (7)	−0.00035 (8)	−0.00013 (6)
C^{123}	0.00040 (8)	0.00012 (4)	0.00013 (5)	−0.00012 (5)
C^{133}	0.00061 (11)	−0.00024 (5)	−0.00057 (7)	0.00014 (7)
C^{222}	0.0018 (2)	−0.00080 (8)	−0.00010 (8)	−0.00017 (7)
C^{223}	0.00114 (13)	0.00009 (4)	0.00004 (5)	−0.00009 (4)
C^{233}	0.00116 (13)	−0.00017 (5)	−0.00010 (5)	0.00016 (5)
C^{333}	0.0022 (2)	−0.00021 (9)	0.00014 (10)	−0.00008 (10)

volumes (within the s.u.), that the symmetry was higher than monoclinic. Indeed, the atomic positions fulfilled the trigonal symmetry, space group $P321$. In this space group the refinement smoothly converged toward the residual $R = 0.068$ value [$2\sigma(I)$ cut-off for observed reflections, all reflections included in the refinement], with the $Ag_{15}CuSb_2S_{11}$ stoichiometry, full site occupancy, one split position (S10, very close to, but not on, the threefold axis) and a mirror twin operation (first-degree twin, $\bar{3}'2/m'1$ polychromatic point group). However, large positive residues (up to 4 e Å^{-3}) were observed almost on top of all the heavy atoms of the $[(Ag,Cu)_6Sb_2S_7]^{2-}$ A pseudo layer (see §4) and in the vicinity of Ag atoms of the $[Ag_9CuS_4]^{2+}$ B pseudo layer. These residues could be taken into account in the monoclinic symmetry by introducing a stacking fault, that is, the presence of a minor component (∼10%) related to the cell content by an inversion centre (introduced in *JANA*2000 with rigid bodies), but not by the introduction of an inversion twin law. However, without any significant residues left in the difference Fourier synthesis maps, the correlations were still very high and did not allow the refinement convergence (even with a very small damping factor).

A new data collection was then performed on the same crystal and the same diffractometer at 120 K. Surprisingly, the refinement largely improved in the trigonal symmetry, space group $P321$, with a residual R value of 0.0423 and without the presence of significant positive residues in the difference Fourier synthesis. Adding non-harmonic terms for Ag6, Ag8 and Ag10 in the $[Ag_9CuS_4]^{2+}$ B pseudo layer and for Ag3 coordinated by the split S10 position, R further dropped to 0.0387. Allowing a Cu/Ag mixed occupation of the Ag sites in the $[(Ag,Cu)_6Sb_2S_7]^{2-}$ A pseudo layer, introducing a secondary extinction coefficient (Becker & Coppens, 1974), and taking into account the inversion twin ($\bar{3}'2/m'1$ polychromatic point group), the final residual value was $R = 0.0359$ ($wR = 0.0448$) for 6224 independent observed reflections [$2\sigma(I)$ level] and 224 parameters and $R = 0.0450$ ($wR = 0.0458$) for all 6847 independent reflections. Crystal characteristics, data collection and reduction parameters, and refinement results are gathered in Table 2. Atomic parameters are available in the supplementary data and in Table 3.

Note that all attempts to lift the disorder in the 221 structure (observed on atom S10) by introducing additional twin laws and/or changing symmetry failed. It is also worth noticing that a third data collection performed after returning to room temperature led to results comparable with those obtained from the first room-temperature data set, that is, with positive residues corresponding to the inverted structure (in the monoclinic cell), which could be explained by a stacking fault but not by an inversion twin law.

4. Structure description

4.1. 222-Polybasite

To make the description easier, the 222-polybasite structure can be seen as a succession along the c axis of two module layers: the $[(Ag,Cu)_6Sb_2S_7]^{2-}$ A (or A') module layer and the $[Ag_9CuS_4]^{2+}$ B (or B') module layer (A/B and A'/B' being related by a c-glide-mirror symmetry operation, see Fig. 1). The analysis of each module cannot be made independently, however, since some atoms have coordinating atoms in the other module.

As is usually the case when dealing with d^{10} cations, such as Ag^+ or Cu^+, the structure description in terms of simple polyhedra is not possible. Indeed, for such cations there is no clear cut difference between the bonding and non-bonding distances since the coordinating atoms are at distances which span a large interval, defining highly distorted polyhedra with preferentially low-coordination d^{10} environments. Gaudin *et al.* (2001) pointed out by means of FLAPW (full potential linearized augmented plane wave) band-structure calculations that the factors influencing the low coordination are the metal s/d orbital mixing and the d^{10} element polarization. Since the coordination number cannot be straightforwardly given as an integer number, the solution consists of using the weighted mean distance, $\langle {}^n d(ij \rightarrow r)\rangle$, hereafter referred to as ^{n}WMD,

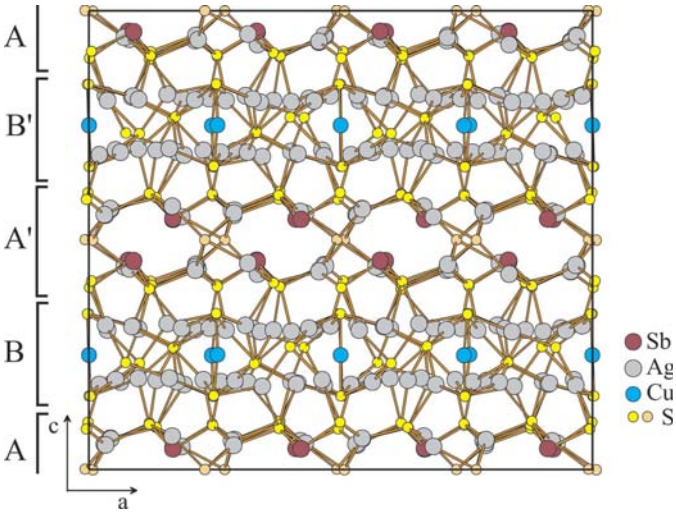

Figure 1
Projection of the 222-polybasite structure along the monoclinic *b* axis, emphasizing the succession of the $[(Ag,Cu)_6Sb_2S_7]^{2-}$ *A* (*A*′) and $[Ag_9CuS_4]^{2+}$ *B* (*B*′) module layers. Atoms Ag13 and Ag14 are highlighted (different colour) for comparison with Figs. 2 and 3.

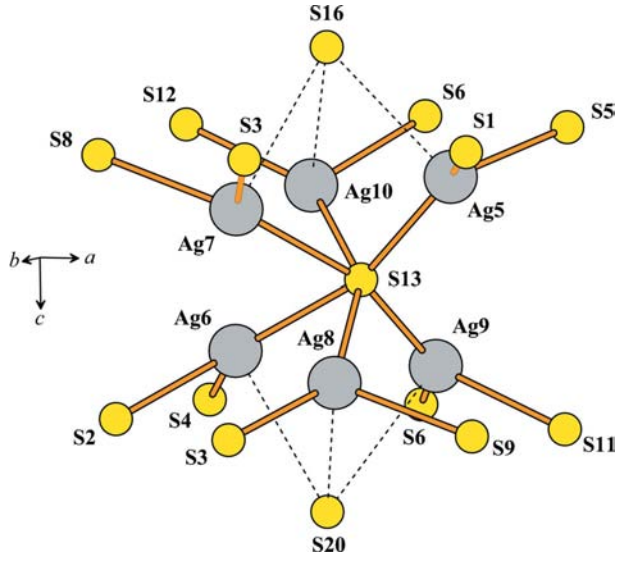

Figure 2
The threefold coordination of Ag in the $[(Ag,Cu)_6Sb_2S_7]^{2-}$ *A* (*A*′) module layer and the connection between the $[AgS_3]^{5-}$ triangular units (arrangement valid for both the 222- and 221-polybasite structures, labelling for the 222-structure only). Although not in the *A* (*A*′) module layer, S16 and S20 at longer Ag—S distances are included for completeness.

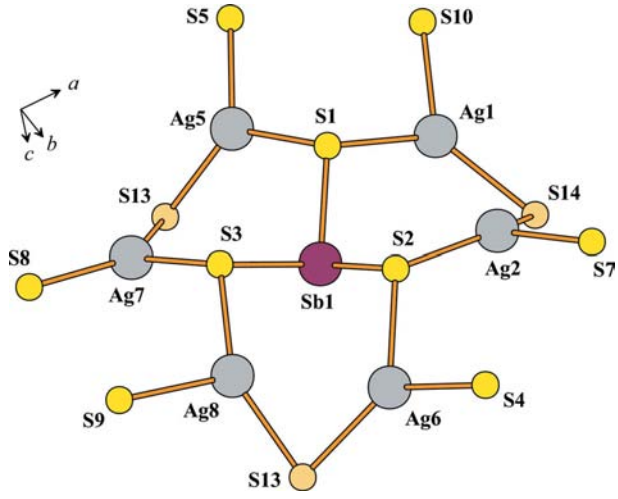

Figure 3
The connection between the $[AgS_3]^{5-}$ triangular units and the $[SbS_3]^{3-}$ pyramid in the $[(Ag,Cu)_6Sb_2S_7]^{2-}$ *A* (*A*′) module layer (arrangement valid for both the 222- and 221-polybasite structures, labelling for the 222-structure only).

and the effective coordination number, ^{n}ECoN, as defined by Hoppe (1979) and Nespolo *et al.* (2001), obtained through the scaling of each bond distance to the shortest bond length of each polyhedron (instead of an empirical normalization parameter used in the classical bond valence analysis). These parameters have been calculated for each cation using the *Chardi-IT* program (Nespolo *et al.*, 2001) and are gathered in Table 4, along with interatomic distances calculated using the *JANA*2000 program. Notice that the charge distribution could not be calculated for the 222-polybasite structure since the *Chardi-IT* program cannot handle a large number of independent atoms in its present version. The charge distribution was, however, calculated for the 221-polybasite structure. It shows a very good agreement with the standard oxidation states (see below), which suggests that the results would be even better for the 222-polybasite phase since its structure is less disordered.

In the $[(Ag,Cu)_6Sb_2S_7]^{2-}$ *A* (or *A*′) module layer each silver cation has a sulfur threefold coordination (see Figs. 2 and 3), although slightly out of the S3 triangle and establishing a very weak bond with an additional S atom (as shown in Table 4 with ^{n}ECoN values greater than 3.0). Each $[AgS_3]^{5-}$ unit is linked either to five other $[AgS_3]^{5-}$ units by sharing a common sulfur apex (see Fig. 2), as copper does in $Cu_{12}Sb_4S_{13}$ (Pfitzner *et al.*, 1997), or to a single $[AgS_3]^{5-}$ unit and a $[SbS_3]^{3-}$ pyramid (see Fig. 3). Out of the 12 independent Ag atoms of the *A* module layer, only one atom (*e.g.* Ag3) exhibits significantly shorter Ag—S distances [2.381 (3), 2.408 (3) and 2.429 (3) Å] and a weighted mean distance [2.416 Å compared with the 2.53 (3) Å average value calculated for the other Ag atoms], as easily shown by a Grubbs test for outliers (Grubbs, 1969). It is on this particular site (Ag3) that a partial replacement of silver by copper was carried out in the refinement process. In the $[SbS_3]^{3-}$ pyramid the mean ⟨Sb—S⟩ bond distance [2.422 (14) Å] is equal to the average ^{n}WMD [2.422 (6) Å] and is consistent with the value obtained by considering the ⟨Sb—S⟩ bonds of pyrargyrite, $Ag_3[SbS_3]$ (2.452 Å; Engel & Nowacki, 1966).

In the $[Ag_9CuS_4]^{2+}$ *B* (or *B*′) module layer, the 18 independent Ag atoms adopt various coordinations extending from quasi-linear to quasi-tetrahedral (see Fig. 4). These coordinations are very well characterized by their ^{n}ECoN value, ranging from 1.997 to 3.883. Seven Ag atoms (*i.e.* Ag13, Ag15, Ag19, Ag21, Ag22, Ag23 and Ag28) have ^{n}ECoN values close to 2.0 (from 1.997 to 2.127) and can be considered in linear coordination with ⟨Ag—S⟩ = 2.44 (3) Å, although the

Table 4
Main interatomic distances (Å) and s.u.s, weighted mean distance (Å), ^{n}ECoN and charge distribution for the selected 222- and 221-polybasite crystals.

For charge distribution, see definitions given by Hoppe (1979) and Nespolo *et al.* (2001).

222-Polybasite (100 K)					
$[(Ag,Cu)_6Sb_2S_7]^{2-}$ *A* (*A*′) layer					
Sb1—S1	2.408 (2)	Sb2—S4	2.409 (2)		
Sb1—S2	2.413 (2)	Sb2—S6	2.421 (2))		
Sb1—S3	2.426 (2)	Sb2—S5	2.432 (2)		
$\langle^2 d\rangle$	2.415	$\langle^2 d\rangle$	2.420		
^{2}ECoN	2.999	^{2}ECoN	2.998		
Sb3—S12	2.411 (2)	Sb4—S11	2.416 (2)		
Sb3—S8	2.412 (2)	Sb4—S10	2.430 (2)		
Sb3—S7	2.453 (2)	Sb4—S9	2.439 (2)		
$\langle^2 d\rangle$	2.424	$\langle^2 d\rangle$	2.428		
^{2}ECoN	2.993	^{2}ECoN	2.998		
Ag1—S1	2.520 (2)	Ag2—S2	2.461 (2)	Ag3/Cu—S14	2.381 (3)
Ag1—S10	2.556 (2)	Ag2—S14	2.489 (3)	Ag3/Cu—S7	2.408 (3)
Ag1—S14	2.569 (3)	Ag2—S7	2.584 (2)	Ag3/Cu—S4	2.429 (3)
Ag1—S17	3.0732 (19)	Ag2—S17	2.953 (2)	Ag3/Cu—S21	3.013 (2)
$\langle^3 d\rangle$	2.569	$\langle^4 d\rangle$	2.532	$\langle^3 d\rangle$	2.416
^{3}ECoN	3.289	^{4}ECoN	3.372	^{3}ECoN	3.142
Ag4—S10	2.492 (2)	Ag5—S1	2.449 (2)	Ag6—S4	2.530 (2)
Ag4—S14	2.513 (3)	Ag5—S5	2.470 (2)	Ag6—S2	2.531 (2)
Ag4—S5	2.597 (2)	Ag5—S13	2.474 (2)	Ag6—S13	2.562 (2)
Ag4—S21	3.0915 (18)	Ag5—S16	2.959 (2)	Ag6—S20	3.0490 (19)
$\langle^3 d\rangle$	2.547	$\langle^3 d\rangle$	2.487	$\langle^3 d\rangle$	2.564
^{3}ECoN	3.204	^{3}ECoN	3.320	^{3}ECoN	3.322
Ag7—S8	2.513 (2)	Ag8—S3	2.466 (2)	Ag9—S6	2.442 (2)
Ag7—S3	2.548 (2)	Ag8—S13	2.496 (2)	Ag9—S13	2.482 (2)
Ag7—S13	2.566 (2)	Ag8—S9	2.614 (2)	Ag9—S11	2.611 (2)
Ag7—S16	3.112 (2)	Ag8—S20	3.0220 (19)	Ag9—S20	3.210 (2)
$\langle^3 d\rangle$	2.559	$\langle^4 d\rangle$	2.538	$\langle^3 d\rangle$	2.506
^{3}ECoN	3.223	^{4}ECoN	3.257	^{3}ECoN	2.997
Ag10—S12	2.499 (2)	Ag11—S9	2.516 (2)	Ag12—S11	2.453 (3)
Ag10—S13	2.535 (2)	Ag11—S14	2.536 (3)	Ag12—S14	2.481 (3)
Ag10—S6	2.577 (2)	Ag11—S8	2.579 (2)	Ag12—S12	2.525 (3)
Ag10—S16	3.121 (2)	Ag11—S21	3.0306 (19)	Ag12—S17	3.290 (3)
$\langle^3 d\rangle$	2.550	$\langle^3 d\rangle$	2.567	$\langle^2 d\rangle$	2.487
^{3}ECoN	3.190	^{3}ECoN	3.345	^{2}ECoN	3.019
$[Ag_9CuS_4]^{2+}$ *B* (*B*′) layer (in increasing ^{n}ECoN for Ag)					
Cu1—S17	2.1572 (17)	Cu2—S21	2.1549 (16)	Cu3—S20	2.164 (2)
Cu1—S17	2.1572 (17)	Cu2—S21	2.1549 (16)	Cu3—S16	2.171 (2)
$\langle^1 d\rangle$	2.157	$\langle^1 d\rangle$	2.155	$\langle^2 d\rangle$	2.168
^{1}ECoN	2.000	^{1}ECoN	2.000	^{2}ECoN	2.000
Ag22—S15	2.410 (2)	Ag13—S15	2.425 (2)	Ag15—S19	2.3992 (19)
Ag22—S9	2.442 (2)	Ag13—S16	2.488 (2)	Ag15—S7	2.414 (2)
$\langle^2 d\rangle$	2.425	$\langle^2 d\rangle$	2.456	$\langle^2 d\rangle$	2.407
^{2}ECoN	1.997	^{2}ECoN	1.998	^{2}ECoN	1.999
Ag28—S18	2.420 (2)	Ag21—S18	2.4277 (19)	Ag19—S19	2.4363 (19)
Ag28—S5	2.424 (2)	Ag21—S20	2.483 (2)	Ag19—S17	2.490 (2)
		Ag21—S3	3.254 (2)	Ag19—S7	3.197 (2)
		Ag21—S9	3.272 (2)		
$\langle^2 d\rangle$	2.422	$\langle^3 d\rangle$	2.462	$\langle^3 d\rangle$	2.471
^{2}ECoN	2.000	^{3}ECoN	2.057	^{3}ECoN	2.066
Ag23—S19	2.4395 (19)	Ag18—S18	2.460 (2)	Ag27—S15	2.465 (2)
Ag23—S21	2.484 (2)	Ag18—S21	2.477 (2)	Ag27—S21	2.506 (2)
Ag23—S4	3.114 (2)	Ag18—S8	2.849 (2)	Ag27—S10	2.846 (2)
				Ag27—S5	3.287 (2)
$\langle^3 d\rangle$	2.477	$\langle^4 d\rangle$	2.517	$\langle^5 d\rangle$	2.541
^{3}ECoN	2.127	^{4}ECoN	2.567	^{5}ECoN	2.666
Ag30—S17	2.544 (2)	Ag25—S22	2.5240 (18)	Ag29—S22	2.568 (2)
Ag30—S22	2.544 (2)	Ag25—S20	2.537 (2)	Ag29—S16	2.584 (2)

S—Ag—S angles always depart from 180° (with 157.8° as minimum value). The mean ⟨Ag—S⟩ distance is consistent with the average ^{n}WMD of 2.45 (3) Å. Six Ag atoms (*i.e.* Ag19, Ag24, Ag25 Ag27, Ag29 and Ag30) may be considered as threefold coordinated (^{n}ECoN values in the range 2.567–3.455), even though some of them are in a 2 short + 1 long bond distance environment. Taking into account three bonds per atom, a mean Ag—S of 2.59 (11) Å can be calculated, that is consistent with the average ^{n}WMD = 2.57 (4) Å and significantly different from the average ^{n}WMD calculated for the linear coordination. The calculated average Ag—S distance for a threefold coordination is in good agreement with both that found for the Ag(1) position in the crystal structure of stephanite, $Ag_5[S|SbS_3]$ (2.54 Å; Ribár & Nowacki, 1970) and that found for the Ag position in the crystal structure of pyrargyrite, $Ag_3[SbS_3]$ (2.573 Å; Engel & Nowacki, 1966). The last five Ag atoms (*i.e.* Ag14, Ag16, Ag17, Ag20, Ag26) adopt a close-to-tetrahedral coordination, with $3.707 \leq {}^n\text{ECoN} \leq 3.883$. Once again, taking only four bonds for the averaging, one calculates ⟨Ag—S⟩ = 2.70 (14) Å which matches the calculated average ^{n}WMD = 2.668 (14) Å. This average bond distance is in excellent agreement with that found for the Ag3 position in the crystal structure of stephanite, $Ag_5[S|SbS_3]$ (2.68 Å; Ribár & Nowacki, 1970). Finally, the three Cu atoms show 'true' linear coordinations with similar Cu—S distances [⟨Cu—S⟩ = 2.160 (6) Å]. These distances are in good agreement with those found in KCuS (2.129 and 2.162 Å; Savelsberg & Schäfer, 1978; where Cu2 shows a similar sulfur linear coordination). It is worth noting that the shortest Ag—Ag and Ag—Cu contacts [2.9324 (18) and 2.7752 (12) Å, respectively] are slightly longer than those found in pure metal (Ag 2.89 Å) or deduced from the metal radii (Ag—Cu 2.72 Å).

The refined composition, $Ag_{14.81}Cu_{1.19}Sb_2S_{11}$, is in reasonably good agreement with that obtained through the chemical analysis: $(Ag_{14.48}Cu_{1.29})_{\Sigma=15.77}Sb_{1.98}S_{11.14}$, neglecting the minor Pb, Bi and As components. It can be noted that the apparent minor content of copper observed in the refined composition could be corrected by substituting more Ag by Cu on the 12 independent Ag sites of the

Table 4 (continued)

222-Polybasite (100 K)					
Ag30—S12	2.688 (2)	Ag25—S11	2.659 (2)	Ag29—S6	2.587 (2)
				Ag29—S18	3.432 (2)
$\langle^2d\rangle$	2.582	$\langle^2d\rangle$	2.565	$\langle^2d\rangle$	2.583
^{2}ECoN	2.939	^{2}ECoN	2.945	^{2}ECoN	3.030
Ag24—S18	2.523 (2)	Ag17—S22	2.5872 (18)	Ag20—S22	2.5463 (17)
Ag24—S4	2.607 (3)	Ag17—S3	2.613 (2)	Ag20—S2	2.600 (2)
Ag24—S20	2.654 (2)	Ag17—S16	2.685 (2)	Ag20—S20	2.723 (2)
Ag24—S19	3.101 (3)	Ag17—S18	2.923 (2)	Ag20—S19	2.8674 (19)
Ag24—S6	3.261 (3)				
$\langle^5d\rangle$	2.625	$\langle^4d\rangle$	2.663	$\langle^4d\rangle$	2.648
^{5}ECoN	3.455	^{4}ECoN	3.707	^{4}ECoN	3.721
Ag16—S1	2.594 (2)	Ag26—S15	2.529 (2)	Ag14—S19	2.562 (2)
Ag16—S22	2.6115 (19)	Ag26—S17	2.611 (2)	Ag14—S16	2.628 (3)
Ag16—S17	2.798 (2)	Ag26—S10	2.745 (2)	Ag14—S8	2.707 (3)
Ag16—S15	2.840 (2)	Ag26—S11	2.911 (2)	Ag14—S12	2.964 (3)
		Ag26—S15	3.219 (2)	Ag14—S18	3.231 (3)
$\langle^3d\rangle$	2.682	$\langle^6d\rangle$	2.666	$\langle^6d\rangle$	2.680
^{3}ECoN	3.766	^{6}ECoN	3.879	^{6}ECoN	3.883
Shortest cation–cation distances: Ag—Cu 2.7752 (12), Ag—Ag 2.9324 (18), Ag—Sb 3.311 (2) Å					
221-polybasite (120 K)					
$[(Ag,Cu)_6Sb_2S_7]^{2-}$ *A* layer					
Sb1—S1	2.413 (2)	Sb2—S4	2.4095 (16)	Ag1—S3	2.5324 (18)
Sb1—S1	2.413 (2)	Sb2—S3	2.422 (2)	Ag1—S1	2.537 (2)
Sb1—S1	2.413 (2)	Sb2—S2	2.4392 (15)	Ag1—S9	2.556 (2)
				Ag1—S5	3.0680 (14)
$\langle^1d\rangle$	2.413	$\langle^2d\rangle$	2.423	$\langle^3d\rangle$	2.563
^{1}ECoN	3.000	^{2}ECoN	2.997	^{3}ECoN	3.296
Q	3.043	*Q*	2.973	*Q*	1.015
q/*Q*	0.986	*q*/*Q*	1.009	*q*/*Q*	0.985
Ag2/Cu—S1	2.4133 (18)	Ag3/Cu†—S10	2.4015	Ag4—S4	2.4786 (18)
Ag2/Cu—S9	2.437 (3)	Ag3/Cu—S3	2.497 (3)	Ag4—S9	2.502 (3)
Ag2/Cu—S2	2.4810 (19)	Ag3/Cu—S2	2.486 (2)	Ag4—S4	2.609 (2)
Ag2/Cu—S5	2.977 (2)	Ag3/Cu—S6	3.030 (3)	Ag4—S5	3.1633 (18)
$\langle^3d\rangle$	2.460	$\langle^4d\rangle$	2.472	$\langle^3d\rangle$	2.533
^{3}ECoN	3.235	^{4}ECoN	3.170	^{3}ECoN	3.092
Q	1.006	*Q*	0.962	*Q*	0.996
q/*Q*	0.995	*q*/*Q*	1.039	*q*/*Q*	1.004
$[Ag_9CuS_4]^{2+}$ *B* layer (in increasing ^{n}ECoN for Ag)					
Cu1—S5	2.1663 (13)	Cu2—S6	2.152 (2)		
Cu1—S5	2.1663 (13)	Cu2—S6	2.152 (2)		
$\langle^1d\rangle$	2.166	$\langle^1d\rangle$	2.152		
^{1}ECoN	2.000	^{1}ECoN	2.000		
Q	1.033	*Q*	1.059		
q/*Q*	0.968	*q*/*Q*	0.945		
Ag6—S7	2.4065 (18)	Ag9—S7	2.429 (2)	Ag7—S7	2.4552 (17)
Ag6—S2	2.425 (2)	Ag9—S5	2.490 (3)	Ag7—S6	2.4891 (8)
		Ag9—S2	3.2822 (17)	Ag7—S3	2.9156 (17)
$\langle^2d\rangle$	2.415	$\langle^3d\rangle$	2.463	$\langle^4d\rangle$	2.516
^{2}ECoN	1.999	^{3}ECoN	2.029	^{4}ECoN	2.450
Q	0.979	*Q*	1.004	*Q*	1.017
q/*Q*	1.021	*q*/*Q*	0.996	*q*/*Q*	0.983
Ag8—S8	2.5442 (16)	Ag10—S7	2.533 (2)	Ag5—S8	2.5800 (18)
Ag8—S5	2.546 (3)	Ag10—S5	2.6192 (18)	Ag5—S1	2.6058 (17)
Ag8—S4	2.638 (3)	Ag10—S3	2.704 (2)	Ag5—S5	2.744 (2)
		Ag10—S4	3.028 (3)	Ag5—S7	2.8747 (14)
		Ag10—S7	3.252 (3)		
$\langle^2d\rangle$	2.572	$\langle^6d\rangle$	2.656	$\langle^4d\rangle$	2.668
^{2}ECoN	2.974	^{6}ECoN	3.650	^{4}ECoN	3.744
Q	1.000	*Q*	1.004	*Q*	1.003
q/*Q*	1.000	*q*/*Q*	0.996	*q*/*Q*	0.997
Shortest cation–cation distances: Ag—Cu 2.7868 (11) Å, Ag—Ag 2.9227 (9) Å, Ag—Sb 3.4327 (9) Å					

† Values calculated with S10 in the (0,0,0) average position.

$[(Ag,Cu)_6Sb_2S_7]^{2-}$ *A* (or *A*′) module layer. However, such additional substitutions are not justified by the structure analysis and/or refinement results. Ag3, indeed, is the only obvious site which accommodates Cu, showing anomalously low Ag—S distances.

4.2. 221-Polybasite

The structure of 221-polybasite (Fig. 5) is obtained from the 222-polybasite structure by selecting half its cell content along the *c* axis, that is either the *A*–*B* (or *A*′–*B*′) double module layer or the *A*/2–*B*–*A*′/2 (or *A*′/2–*B*′–*A*/2) double module layer since, as already stated in the structure refinement paragraph, *A* and *A*′ are approximately related by a 1/2 translation along the *c* axis. The selected double module layer approximately conforms to a trigonal symmetry, space group *P*321, except for one S atom (S14), which therefore appears as disordered (S10, just off of the threefold axis) in the 221-polybasite structure. This disorder has already been observed in pearceite (Bindi *et al.*, 2006) and could be modelled either with one position and non-harmonic terms (at 300 K) or with a split-atom model (at 120 and 15 K). Although not clearly understood, the origin of the shift of those S atoms by ∼0.5 Å could be linked to the silver preference for threefold out-of-plane coordinations. The good matching between the two structures is illustrated in Figs. 6(*a*) and 6(*b*).

The S10 splitting, introduced in the refinement of the 221-polybasite structure, yields unrealistic Ag3—S10 distances [2.088 (6), 2.462 (8) and 2.756 (7) Å]. To calculate reasonable charge distribution values, the S10 average position was considered instead of the refined one (see Table 4). With that approximation, values reasonably close to 1 are calculated for $q(ij)/Q(ij)$ [with $q(\mathrm{Ag}) = q(\mathrm{Cu}) = 1$, $q(\mathrm{Sb}) = 3$ and $q(\mathrm{S}) = -2$], the largest departure from 1.0 (0.945 and 1.039) being related to the Ag3/Cu and S10 disorders.

The calculated cation-to-sulfur distances compare very well with those obtained for the 222-polybasite structure. For instance, $\langle \mathrm{Sb—S}\rangle_{221} = 2.418\ (11)$ Å matches the $\langle \mathrm{Sb—S}\rangle_{222} = 2.422\ (14)$ Å value obtained for the 222 structure. Similarly, in the $[Ag_9CuS_4]^{2+}$ *B* module layer, $\langle \mathrm{Cu—S}\rangle_{221} = 2.159\ (8)$ Å is equivalent to $\langle \mathrm{Cu—S}\rangle_{222} = 2.160\ (6)$ Å. We also find two Ag atoms (*i.e.* Ag6 and Ag9) in

a quasi-linear coordination [$\langle Ag-S\rangle_{221}$ = 2.44 (4) Å *versus* $\langle Ag-S\rangle_{222}$ = 2.44 (3) Å], two Ag atoms (Ag7 and Ag8) in a close to triangular coordination [$\langle Ag-S\rangle_{221}$ = 2.60 (17) Å *versus* $\langle Ag-S\rangle_{222}$ = 2.59 (11) Å] and finally two Ag atoms (Ag5 and Ag10) in approximately a tetrahedral coordination [$\langle Ag-S\rangle_{221}$ = 2.71 (17) Å *versus* $\langle Ag-S\rangle_{222}$ = 2.70 (14) Å], with mean $\langle Ag-S\rangle$ distances, average ^{n}WMD(Ag→S) and average ^{n}ECoN(Ag→S) matching the corresponding values calculated in the 222 structure.

Apart from the cell and symmetry change and the consequent S10 splitting, the noticeable structure difference compared with the 222-polybasite structure is the higher Ag/Cu substitution, which gives a refined chemical formula, $Ag_{14.52}Cu_{1.48}Sb_2S_{11}$, reasonably close to the chemical analysis formulation: $(Ag_{14.27}Cu_{1.69})_{\Sigma=15.96}Sb_{1.99}S_{10.77}$, neglecting the minor Zn, Bi, As and Se components. As for the 222-polybasite structure, the Ag/Cu mixed sites are located in the $[(Ag,Cu)_6Sb_2S_7]^{2-}$ *A* layer and correspond to the shortest ^{n}WMD (2.460 and 2.472 Å to be compared with 2.533 and 2.563 Å for an Ag full site occupation).

4.3. Polytypism and disorder

The 222-polybasite structure with the *–AB–A′B′–AB–A′B′–* double-layer module sequence can be considered as a polytype of the 221-polybasite structure of sequence *–AB–AB–*, the *A′B′* double layer module being related to *AB* by a glide reflection perpendicular to the *b* axis with translational component **c**/2. However, the AB_{221} module is not strictly equivalent in chemical composition to the AB_{222} (or $A'B'_{222}$) module, the 221-polybasite structure being richer in copper content. It seems that the higher the Cu content, the more likely the structure will be of the 221 type. The question of a 222-polybasite structure with the $Ag_{15}CuSb_2S_{11}$ stoichiometric chemical formula remains.

The minor presence of *–AB–AB–* and/or *–A′B′–A′B′–* sequences in the 222-polybasite structure determined for the crystal from the 17002/38 sample is not excluded. It would explain the need for a specific scale factor for the *hkl*, $l = 2n + 1$, reflections. Conversely, the presence of a *A′B′* double-layer module has been detected in the *–AB–AB–* sequence of the 221-polybasite structure determined at room temperature from the crystal selected in the 2503/I sample. Surprisingly,

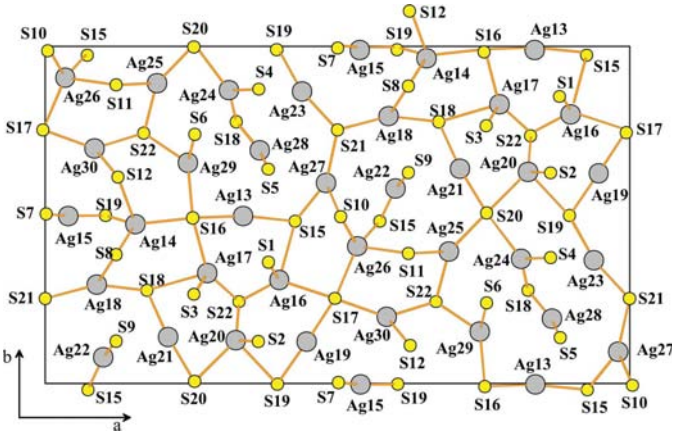

Figure 4
Projection along the *c* axis of a part of the 222-polybasite $[Ag_9CuS_4]^{2+}$ *B* (*B′*) module layer, showing the various coordinations observed for silver.

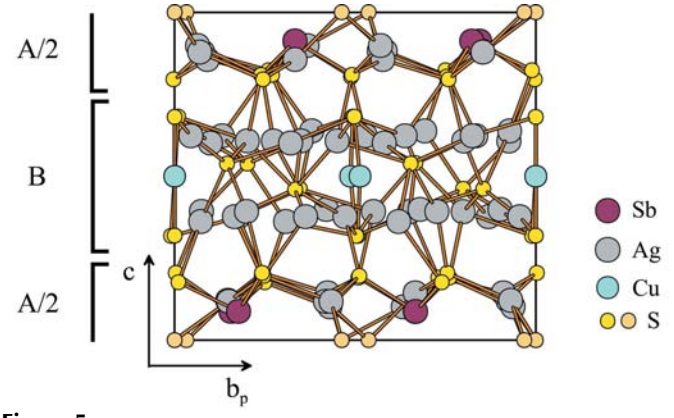

Figure 5
Projection of the 221-polybasite structure along the hexagonal *a* axis.

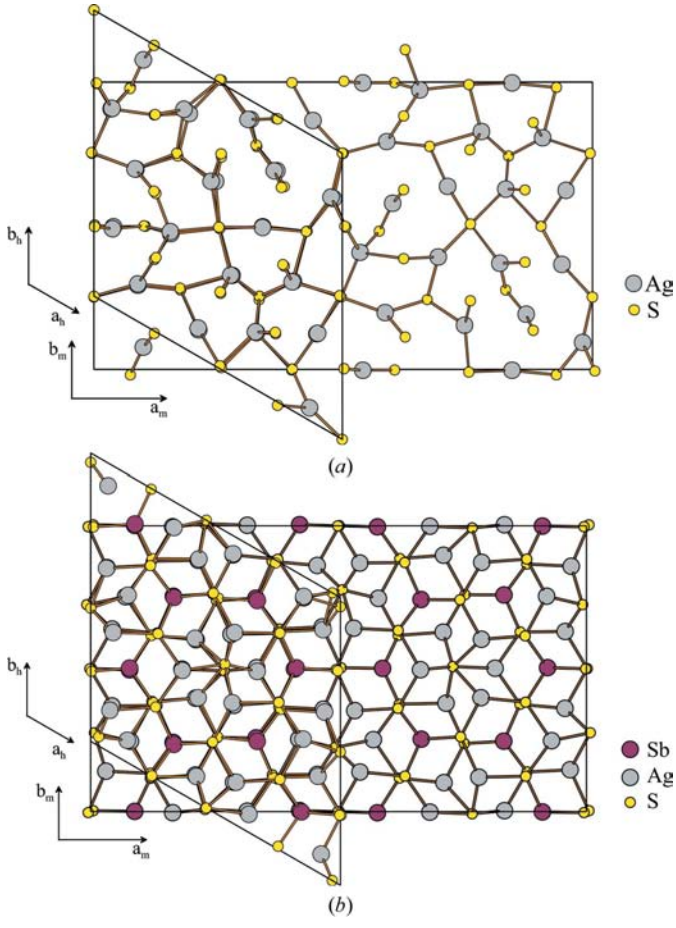

Figure 6
Superposition, down the *c* axis, of equivalent parts of the 222- and 221-polybasite $[(Ag,Cu)_6Sb_2S_7]^{2-}$ *A* (*a*) and $[Ag_9CuS_4]^{2+}$ *B* (*b*) module layers, showing the good matching between two structures.

that insertion disappeared in the low-temperature (120 K) analysis, the lowering of the temperature generating an ordering of the disordered layers. This can, however, be understood when one realizes that the AB to $A'B'$ change is simply achieved by a displacement of the Ag d^{10} cations in the $[Ag_9CuS_4]^{2+}$ B module layer. These displacements, indeed, do not require a large amount of energy since our experiments (currently in progress) showed these compounds to be good ionic conductors down to well below room temperature.

As is generally the case, the higher the disorder, the higher the apparent symmetry. With a low substitution of Cu for Ag, the crystal system is monoclinic with a double c period. However, the AB ($A'B'$) double layer module has a pseudo trigonal symmetry, which explains the twinning and the apparent hexagonal cell. By increasing the substitution of Cu for Ag, the cell doubling along the c direction is lost and the average symmetry becomes trigonal. A further increase of the disorder gives rise to a folding of the cell along the a and b directions as found in the 111-pearceite structure, $P\bar{3}m1$ space group (Bindi *et al.*, 2006). This supports the idea of Hall (1967) who suggested that the variation of Cu content in different samples might be the driving force of different unit-cell orderings.

5. Concluding remarks

The crystal structures of 222- and 221-polybasite have been solved and refined from X-ray diffraction data sets (collected at 100 and 120 K, respectively) from twinned crystals. The complexity of the structure determination of the 222-polybasite structure comes from the apparent trigonal symmetry linked to a second-degree twinning by metric merohedry of the real monoclinic structure. The complexity is further increased by a pseudo translational symmetry of most atoms, with only the Ag atoms of one module layer not fulfilling the pseudo symmetry. The difficulty in the structure determination of the 221-polybasite structure results from a small contribution, at room temperature, of the 222-polybasite structure resulting from stacking faults. Only at low temperature was that complication removed.

With the two well resolved atomic structures in hand, a pattern of the possible mechanisms regulating the ordering has been proposed: starting from the hypothetical stoichiometric and fully ordered $Ag_{15}CuSb_2S_{11}$ 222-polybasite structure, with a low $C2/c$ monoclinic symmetry and a large 222 supercell, the disorder introduced by the substitution of Cu for Ag increases the symmetry with a cell reduction along the c axis yielding the 221 supercell and a trigonal crystal system. A further increase of the substitution gives rise to a folding of the cell along the a and b axes and the 111-pearceite structure, space group $P\bar{3}m1$. This mechanism needs to be confirmed, for instance through the elucidation of the antimonpearceite and arsenpolybasite structures which are currently in progress.

The authors are grateful to Professor Paul G. Spry (Iowa State University, USA) for his help in electron microprobe analyses. This work was funded by CNR (Istituto di Geoscienze e Georisorse, sezione di Firenze) and by MIUR, PRIN 2005 project 'Complexity in minerals: modulation, modularity, structural disorder'.

References

Becker, P. J. & Coppens, P. (1974). *Acta Cryst.* A**30**, 129–147.
Bindi, L. & Cipriani, C. (2004*a*). *Can. Miner.* **42**, 1269–1274.
Bindi, L. & Cipriani, C. (2004*b*). *Can. Miner.* **42**, 1275–1279.
Bindi, L. & Cipriani, C. (2004*c*). *Am. Miner.* **89**, 1505–1509.
Bindi, L., Evain, M. & Menchetti, S. (2006). *Acta Cryst.* B**62**, 212–219.
Bindi, L. & Pratesi, G. (2005). *Can. Miner.* **43**, 1373–1377.
Bindi, L., Spry, P. G. & Cipriani, C. (2004). *Am. Miner.* **89**, 1043–1047.
Boucher, F., Evain, M. & Brec, R. (1992). *J. Solid State Chem.* **100**, 341–355.
Boucher, F., Evain, M. & Brec, R. (1993). *J. Solid State Chem.* **107**, 332–346.
Brandenburg, K. (2001). *Diamond* (Version 3). Crystal Impact GbR, Bonn, Germany.
Edenharter, A., Koto, K. & Nowacki, W. (1971). *Neues Jahr. Miner. Monatsh.* pp. 337–341.
Engel, P. & Nowacki, W. (1966). *Neues Jahr. Miner. Monatsh.* pp. 181–195.
Evain, M., Gaudin, E., Boucher, F., Petrícek, V. & Taulelle, F. (1998). *Acta Cryst.* B**54**, 376–383.
Frondel, C. (1963). *Am. Miner.* **48**, 565–572.
Gaudin, E., Boucher, F. & Evain, M. (2001). *J. Solid State Chem.* **160**, 212–221.
Gaudin, E., Petrícek, V., Boucher, F., Taulelle, F. & Evain, M. (2000). *Acta Cryst.* B**56**, 972–979.
Grubbs, F. (1969), *Technometrics*, **11**, 1–21.
Hall, H. T. (1967). *Am. Miner.* **52**, 1311–1321.
Harris, D. C., Nuffield, E. W. & Frohberg, M. H. (1965). *Can. Miner.* **8**, 172–184.
Herrendorf, W. (1993). PhD dissertation. University of Karlsruhe, Germany.
Hoppe, R. (1979). *Z. Kristallogr.* **150**, 23–52.
Johnson, C. K. & Levy, H. A. (1974). *International Tables for X-ray Crystallography*, edited by J. A. Ibers and W. C. Hamilton, Vol. IV, pp. 311–336. Birmingham: Kynoch Press.
Kuhs, W. F. & Heger, G. (1979). *Fast Ion Transport in Solids*, edited by P. Vashishta, J. N. Mundy & G. K. Shenoy, pp. 233–236. Amsterdam: Elsevier.
Minčeva-Stefanova, I., Bonev, I. & Punev, L. (1979). *Geok. Mineral. Petrol.* **11**, 13–34.
Nespolo, M. (2004). *Z. Kristallogr.* **219**, 57–71.
Nespolo, M. & Ferraris, G. (2001). *Eur. J. Mineral.* **13**, 1035–1045.
Nespolo, M., Ferraris, G., Ivaldi, G. & Hoppe, R. (2001). *Acta Cryst.* B**57**, 652–664.
Peacock, M. A. & Berry, L. G. (1947). *Min. Mag.* **28**, 2–13.
Petricek, V. & Dusek, M. (2000). *JANA*2000, *A Crystallographic Computing System.* Institute of Physics, Academy of Sciences of the Czech Republic, Prague, Czech Republic.
Pfitzner, A., Evain, M. & Petricek, V. (1997). *Acta Cryst.* B**53**, 337–345.
Ribár, B. & Nowacki, W. (1970). *Acta Cryst.* B**26**, 201–207.
Savelsberg, G. & Schäfer, H. (1978). *Z. Naturforsch. Teil B*, **33**, 711–713.
Stoe & Cie (1996). *X-shape*, Version 1.02. Stoe and Cie, Darmstadt, Germany.